JGR Oceans

RESEARCH ARTICLE
10.1029/2024JC021348

Gross Primary Production of Antarctic Landfast Sea Ice: A Model-Based Estimate

P. Wongpan[1], K. M. Meiners[1,2,3], M. Vancoppenolle[4], A. D. Fraser[1], S. Moreau[5,6], B. T. Saenz[7], K. M. Swadling[1,8], and D. Lannuzel[1,3,8]

[1]Australian Antarctic Program Partnership, Institute for Marine and Antarctic Studies, University of Tasmania, Hobart, TAS, Australia, [2]Australian Antarctic Division, Department of Climate Change, Energy, the Environment and Water, Kingston, TAS, Australia, [3]Australian Research Council Australian Centre for Excellence in Antarctic Science, Institute for Marine and Antarctic Studies, University of Tasmania, Hobart, TAS, Australia, [4]Laboratoire d'Océanographie et du Climat, CNRS/IRD/MNHN, Sorbonne Université, Paris, France, [5]Norwegian Polar Institute, Fram Centre, Tromsø, Norway, [6]Department of Geosciences, iC3: Centre for ice, Cryosphere, Carbon and Climate, UiT The Arctic University of Norway, Tromsø, Norway, [7]Biota.earth, Berkeley, CA, USA, [8]Institute for Marine and Antarctic Studies, University of Tasmania, Hobart, TAS, Australia

Abstract Much of the Antarctic coast is covered by seasonal landfast sea ice (fast ice), which serves as an important habitat for ice algae. Fast-ice algae provide a key early season food source for pelagic and benthic food webs, and contribute to biogeochemical cycling in Antarctic coastal ecosystems. Summertime fast ice is undergoing a decline, leading to more seasonal fast ice with unknown impacts on interconnected Earth system processes. Our understanding of the spatiotemporal variability of Antarctic fast ice, and its impact on polar ecosystems is currently limited. Evaluating the overall productivity of fast-ice algae has historically been hampered by limitations in observations and models. By linking new fast-ice extent maps with a one-dimensional sea-ice biogeochemical model, we provide the first estimate of the spatio-seasonal variability of Antarctic fast-ice algal gross primary production (GPP) and its annual primary production on a circum-Antarctic scale. Experiments conducted for the 2005–2006 season provide a mean fast ice-algal production estimate of 2.8 Tg C/y. This estimate represents about 12% of overall Southern Ocean sea-ice algae production (estimated in a previous study), with the mean fast-ice algal production per area being 3.3 times higher than that of pack ice. Our Antarctic fast-ice GPP estimates are probably underestimated in the Ross Sea and Weddell Sea sectors because the sub-ice platelet layer habitats and their high biomass are not considered.

Plain Language Summary Antarctic landfast sea ice (fast ice) is sea ice fastened to the coastline of Antarctica and provides a prolific habitat for microalgae. These ice algae are ecologically important because their production takes place early in the season when water column primary production is low. By combining a new satellite data set and a biogeochemical sea-ice algal growth model, this study provides the first estimate of circum-Antarctic fast-ice algal production: 2.8 million tonnes of carbon per year, which is about 12% of the total Antarctic sea-ice algal production. The mean algal primary production per area in fast ice is 3.3 times higher than that of pack ice.

Key Points:

- First estimate of circum-Antarctic landfast sea-ice annual gross primary production, with a focus on the 2005–2006 season
- Mean landfast sea-ice algal primary production is 2.8 TgC/y, representing 12% (range 5%–19%) of total Southern Ocean ice algal productivity
- Mean modeled landfast sea-ice algal production per area is 3.3 times higher than that of pack ice

Supporting Information:

Supporting Information may be found in the online version of this article.

Correspondence to:

P. Wongpan,
pat.wongpan@utas.edu.edu

Citation:

Wongpan, P., Meiners, K. M., Vancoppenolle, M., Fraser, A. D., Moreau, S., Saenz, B. T., et al. (2024). Gross primary production of Antarctic landfast sea ice: A model-based estimate. *Journal of Geophysical Research: Oceans*, *129*, e2024JC021348. https://doi.org/10.1029/2024JC021348

Received 18 MAY 2024
Accepted 11 SEP 2024

Author Contributions:

Conceptualization: P. Wongpan, K. M. Meiners, M. Vancoppenolle, A. D. Fraser, D. Lannuzel
Data curation: P. Wongpan, A. D. Fraser, B. T. Saenz, K. M. Swadling
Formal analysis: P. Wongpan
Funding acquisition: K. M. Meiners, D. Lannuzel
Investigation: P. Wongpan
Methodology: P. Wongpan, K. M. Meiners, M. Vancoppenolle, A. D. Fraser, D. Lannuzel
Project administration: P. Wongpan, K. M. Meiners, D. Lannuzel
Resources: P. Wongpan, K. M. Meiners, A. D. Fraser, D. Lannuzel

1. Introduction

Much of the Antarctic coast is covered by a belt of landfast sea ice (fast ice), fastened to the land or peripheral ice structures, unlike pack ice which is free drifting (Fraser et al., 2023). Fast ice forms a biogeochemically active barrier that constrains heat, gas and momentum exchanges between the ocean and the atmosphere (Inall et al., 2022; Vancoppenolle et al., 2013) and provides a productive habitat for algal communities. Ice algae provide an early season and highly concentrated food source for Antarctic marine food webs (Kohlbach et al., 2017; Louw et al., 2022). Antarctic fast ice chlorophyll *a* (Chl *a*) concentrations, a proxy for algal biomass, are among the highest recorded in marine ecosystems (Arrigo, 2016; Meiners et al., 2018; Roukaerts et al., 2021). Previous modeling studies have not differentiated between fast ice and pack ice when estimating the Gross Primary Production (GPP) in Antarctic sea ice, despite them being distinctly different habitats. The contribution of fast ice to overall sea ice GPP is thus unclear.

Unlike phytoplankton, sea-ice algal biomass and production cannot be estimated with airborne or spaceborne remote sensing techniques (e.g., DeJong et al., 2018) and in situ observations are limited in space and time, due to

Software: P. Wongpan, M. Vancoppenolle, S. Moreau
Supervision: K. M. Meiners, D. Lannuzel
Validation: P. Wongpan, M. Vancoppenolle
Visualization: P. Wongpan
Writing – original draft: P. Wongpan
Writing – review & editing: P. Wongpan, K. M. Meiners, M. Vancoppenolle, A. D. Fraser, S. Moreau, B. T. Saenz, K. M. Swadling, D. Lannuzel

localized sampling methodologies (Meiners et al., 2017; Pinkerton et al., 2021; Wongpan et al., 2018). Despite sea-ice algae contributing only ∼1% of total Southern Ocean primary production, and 12%–50% of total primary production in the sea-ice zone (Arrigo et al., 1997, 2008; Saenz & Arrigo, 2014), they are ecologically important because their production occurs in locations and at times when algal growth in the water column is limited (Meiners et al., 2018; Quetin et al., 1996). Extrapolating ice-core observations, Legendre et al. (1992) estimated Antarctic sea-ice algal production to be in the range of 63–70 Tg C y^{-1}. More recent modeling studies provide sea-ice GPP estimates ranging between 35.7 Tg C y^{-1} (year 1989–1990, Arrigo et al., 1997) and 23.7 Tg C y^{-1} (year 2005–2006, Saenz & Arrigo, 2014). Over longer time scales, overall Antarctic sea-ice algal production has been estimated to average 15.5 Tg C y^{-1} (157-year mean since 1850, Jeffery et al., 2020), ranging between 11.5 and 19.5 Tg C y^{-1}. Using a novel light transmission index approach, Pinkerton and Hayward (2021) estimated total Antarctic sea-ice GPP to be around 25 Tg C y^{-1}. On a local scale, an East Antarctic field study showed that fast-ice algae contribute 55%–65% to total (pelagic, benthic, and ice-associated (sympagic)) primary production in December (McMinn et al., 2010).

A key constraint for Antarctic sympagic primary production is the areal extent of sea ice (Arrigo et al., 1997), which has experienced significant loss in recent years (Purich & Doddridge, 2023; Raphael & Handcock, 2022). Summertime fast ice is experiencing a decline of its own, profoundly affecting related Earth system processes (Fraser et al., 2023). Despite the critical importance of Antarctic fast ice in a wide variety of coastal processes, we have limited knowledge of its spatial and temporal variability and role in polar ecosystems. Providing a first circum-Antarctic fast-ice extent climatology, Fraser et al. (2021) reported a fast ice contribution (2000–2018) of 4.0%–12.8% of the total sea-ice area (ranging seasonally from 221,000 km^2 in March to 601,000 km^2 in late September/early October). Given the ongoing changes in both overall Southern Ocean sea-ice extent (Fogt et al., 2022; Parkinson, 2019) and, more recently, fast-ice extent (Fraser et al., 2023), a baseline of fast-ice algal production is needed to better understand how changes in fast ice may affect coastal Antarctic ecosystems and associated ecosystem services (Steiner et al., 2021).

This study provides the first estimate of circum-Antarctic fast-ice primary production by linking satellite mapping efforts (Fraser et al., 2020) with a one-dimensional sea-ice biogeochemical model (LIM1D, Vancoppenolle et al., 2010). We focus on 2005–2006 since total and sector-specific primary production in pack ice has been estimated for that year in a previous study (Saenz & Arrigo, 2014). Although Saenz and Arrigo (2014) used a different ice-algal productivity and sea-ice extent product, the structure of our calculations (satellite sea-ice extent driving a 1-dimensional biophysical sea-ice algal productivity model, with common parameterizations) enables a comparison between Antarctic fast-ice and overall Southern Ocean sea-ice productivity. To provide a measure of uncertainty, we also conducted model sensitivity analyses for variations in oceanic heat flux, ice algal silicate half-saturation constant, and snowfall, following suggestions from recent sea-ice algal modeling efforts (Duarte et al., 2017, 2022; Lim et al., 2019; Saenz & Arrigo, 2014).

2. Data and Methods

2.1. One-Dimensional Sea-Ice Biogeochemical Model and Fast-Ice Extent Product

The 1-dimensional Louvain-la-Neuve Sea Ice Model (LIM1D) was configured to model Antarctic fast ice, assumed to form in situ with its spatial distribution prescribed from the recent satellite-derived fast ice product of Fraser et al. (2020), with an initial thickness of 0.05 m (Wongpan et al., 2021), and evolving with a 1–hr time step. LIM1D represents the ice column as 10 layers with equal thickness plus one additional snow layer. Four categories of physical processes are implemented: sea-ice growth and melt, thermal diffusion, brine dynamics, and radiative transfer. Photosynthesis was limited by light and macro-nutrient availability, temperature, and brine salinity. A full description of LIM1D is given in Vancoppenolle et al. (2010), Moreau et al. (2015) and Vancoppenolle and Tedesco (2016). We followed initialization and parameterizations as described in Lim et al. (2019) suggesting that ice algae (represented as diatoms) have higher silicate half-saturation constants (K_{Si}) than pelagic diatom species. The Japanese 55-year atmospheric reanalysis product for driving ocean-sea ice models (JRA55-do; Tsujino et al., 2018) was used as surface forcing (Table S1 in Supporting Information S1), selected because of its high resolution and development for forcing ocean and sea-ice models of the Ocean Model Intercomparison Project Phase 2 (OMIP-2; Tsujino et al., 2020). To avoid truncation of extremely low air temperatures applied in JRA55-do around the Antarctic coast as a function of time and latitude (Large & Yeager, 2004; Tsujino et al., 2018, Figure S1 in Supporting Information S1), JRA55-do temperatures were

Table 1
Sensitivity Experiments

Experiment	Oceanic heat flux	K_{Si} (μM)	Sub-grid -scale snow	Snowfall	Air tem-perature	GPP (Tg C y^{-1})
CONTROL	Constant 0 W m^{-2}	50	Yes	Constant, uniform	ERA5	2.67
OHF	Summer 30 W m^{-2}	50	Yes	Constant, uniform	ERA5	2.58
KSI	Constant 0 W m^{-2}	3.9	Yes	Constant, uniform	ERA5	4.38
OHF_KSI	Summer 30 W m^{-2}	3.9	Yes	Constant, uniform	ERA5	3.97
JRASNOW	Constant 0 W m^{-2}	50	Yes	JRA55-do	ERA5	1.08
JRATEMP[a]	Constant 0 W m^{-2}	50	Yes	Constant, uniform	JRA55-do	2.38
NOSUB	Constant 0 W m^{-2}	50	No	Constant, uniform	ERA5	1.78
Mean (SD)						2.75 (1.26)

Note. K_{Si} is the half-saturation constant of dissolved silica. GPP stands for Gross Primary Production. SD is the standard deviation. OHF is oceanic heat flux. [a]Note that the JRATEMP run is excluded from the Mean and SD calculation.

replaced with data from the fifth-generation European Center for Medium-Range Weather Forecasts re-analysis (ERA5; Hersbach et al., 2018). A simulation (JRATEMP, Table 1) was also performed using the JRA55-do temperatures, despite their unrealistic truncation described above. Selected results from the LIM1D model are shown in Figure 1.

For 2005–2006, fast-ice pixels at a native resolution of 1 km from the satellite-based data set of Fraser et al. (2020) were distributed into 1690 grid cells, matching JRA55-do's 0.5625° grid. Multiyear fast ice (MYI) is abundant in some regions, for example, in Lützow-Holm Bay (Aoki, 2017; Ushio, 2006; Figure 2b). We note that our model

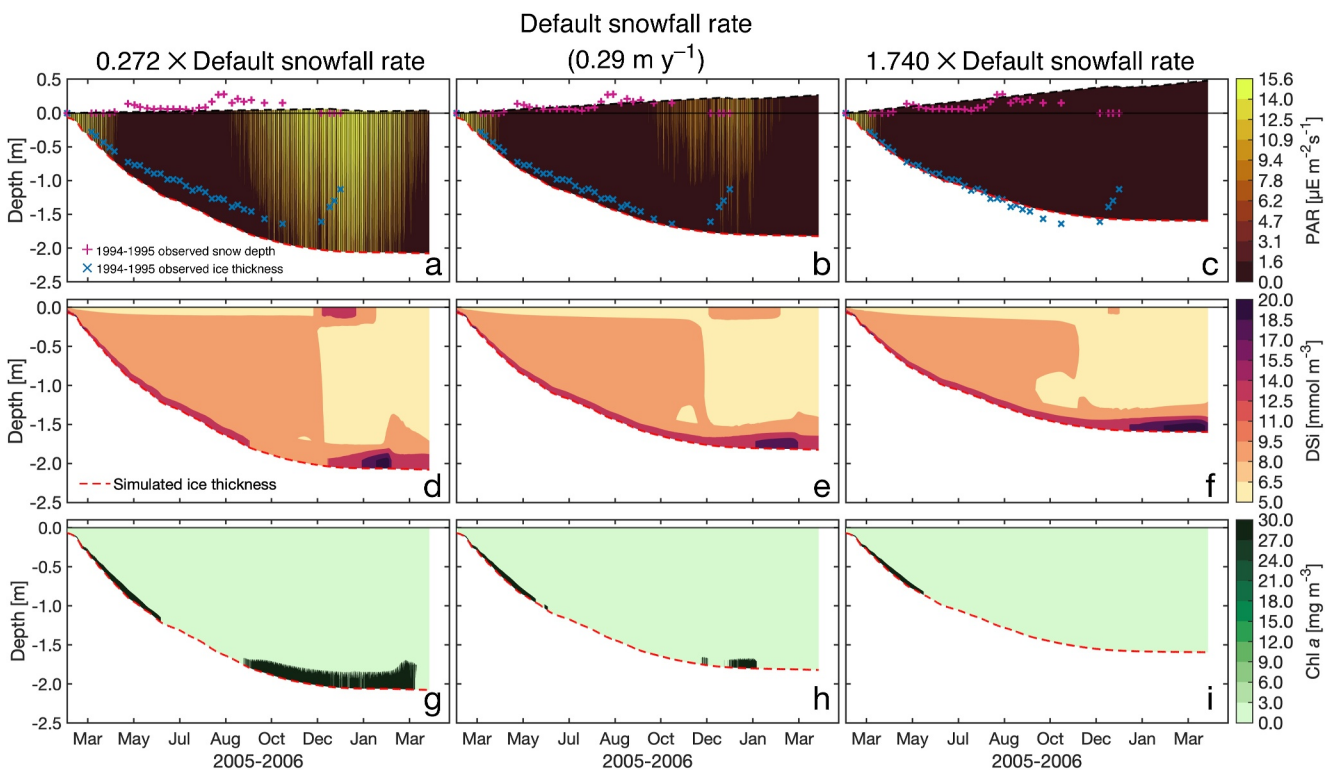

Figure 1. Model evaluation at Davis Station. Evolution of sea-ice and snow depth with contours showing photosynthetically active radiation (PAR) (a–c), dissolved silica (DSi; d–f) and chlorophyll *a* (Chl *a*; g–i) from a grid cell centered at −68.2370°S and 78.1875°E near Davis Station for default snowfall rate (0.29 m y^{-1}, middle), and with 0.272 (left) and 1.740 (right) multipliers. The multipliers are two of the nine multipliers used to simulate a log-normal snow depth distribution (see Table 1 in Saenz & Arrigo, 2014). Note that sea-ice and snow thickness observations are from the 1994–1995 season (Swadling, 1998). Results are shown for the CONTROL run (Table 1). For other runs, please refer to Figures S2–S5 in Supporting Information S1.

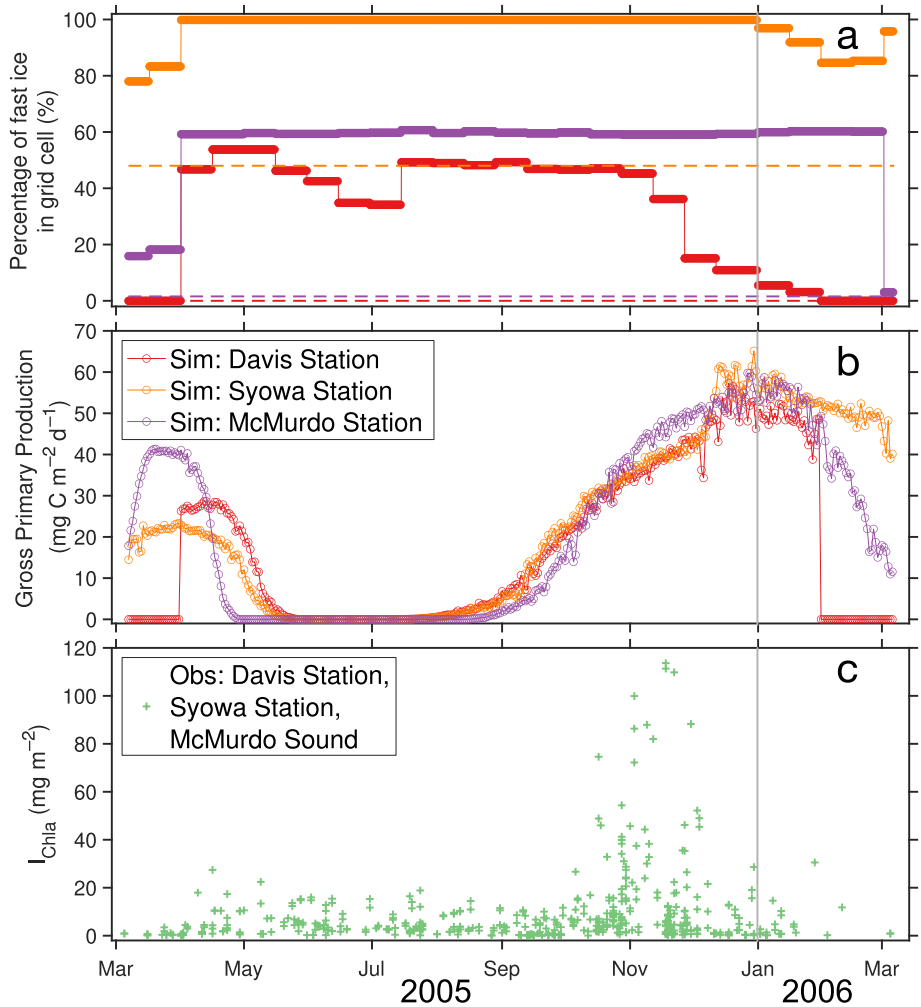

Figure 2. Temporal evolution of (a) records of fast ice percentage (solid lines) for each grid cell. (b) Corresponding daily mean primary production from selected grid cells near Davis Station, Syowa Station and McMurdo Sound and (c) the vertically integrated chlorophyll *a* (Chl *a*) concentrations (I_{Chla}) from observations (Meiners et al., 2018). The dashed lines (in a) represent the multiyear ice fraction for each grid cell, which was not considered in the analysis (Figure 3b). Results show the output for the CONTROL run (Table 1).

configuration only allows for estimating GPP in first-year fast ice (FYI), and that based on annual sampling during 2015–2019 in this region, Chl *a* concentrations in MYI are ∼6 times lower than in FYI (Sahashi et al., 2022). Therefore, we assumed that MYI has relatively low primary productivity compared to FYI and excluded MYI from GPP calculations. Locations of MYI were masked out by analyzing the time series of fast ice cover from the satellite-based data set of Fraser et al. (2020) for 24 months (48 timesteps) within each pixel, from June 2004 to June 2006. A three-point median filter was applied along the time dimension to remove possible errors in a single map. MYI was then defined as a pixel with a (median-filtered) fast ice cover for all time steps.

2.2. Snow Cover, Ocean Heat Flux and Silicate Half-Saturation Sensitivity

As illustrated in Figure 1, snow cover has a large impact on light transmission through the sea ice, thereby strongly influencing sympagic primary production. We performed a range of tests to quantify the effects of varying snow accumulation scenarios on GPP. These can be categorized into three experiments:

1. Spatially uniform, linearly increasing snow cover at a mean rate of 0.29 m y^{-1} (matching the rate observed at a coastal fast ice site (Davis Station) in 1994; Swadling, 1998) but with a log-normal subgrid-scale parameterization of accumulation distribution, following Saenz and Arrigo (2014). For this, each grid cell is divided

into nine equal-area snow depth categories. For each category, snowfall is multiplied by a log-normally distributed, category-specific factor (0.102, 0.272, 0.427, 0.532, 0.721, 0.952, 1.310, 1.740, 3.310), in order to approach a log-normal snow depth distribution (see Table 1 in Saenz & Arrigo, 2014). Finally, primary production in the grid cell is the average of the nine equal-area productivities calculated with different snow depths. This experiment is considered the most realistic approach and is named CONTROL;

2. Snow input directly from JRA55-do (i.e., with spatiotemporally varying snow input)—although this is considered unrealistically heavy (Figure S6 in Supporting Information S1), since many coastal fast-ice regions experience wind-driven snow removal, resulting in a thin snow cover (Fraser et al., 2023). Our model set-up and forcing parameterizations do not include wind-driven snow drift, which is beyond the scope of the present study and will be the focus of future work using a coupled ocean-sea ice-atmosphere model. The present study also includes a prescribed subgrid-scale snow thickness distribution, as above—experiment named JRAS-NOW; and
3. Spatially uniform snow cover increasing linearly throughout the year at a rate of 0.29 m y^{-1} (as with CONTROL), but without subgrid-scale snow thickness distribution—experiment named NOSUB.

Due to a wide range of oceanic heat flux observations (both positive and negative in sign, e.g., Heil et al., 1996; Langhorne et al., 2015) and our model not being coupled to the ocean, we assumed no sensible heat flux from the ocean to the ice (0 W m^{-2}) for the CONTROL run; due to a lack of data on the seasonal changes in regional oceanic heat flux to force the model (e.g., Wongpan et al., 2021). We also conducted experiments with an oceanic heat flux of 30 W m^{-2} during summer (experiment named OHF, Table 1), which was derived from observations at Davis Station (Swadling, 1998; Figure S2 in Supporting Information S1). Davis Station is a suitable area for model evaluation as it is covered by first-year, level fast ice that breaks out entirely in summer (Heil, 2006) and is generally not influenced by ice shelf water, that is, shows no platelet ice accumulation.

We also performed an experiment to test the effect of modified silicate half-saturation constants (KSI) from K_{Si} = 50 μM in the CONTROL experiment (after Lim et al., 2019) to K_{Si} = 3.9 μM in the KSI experiment (after Sarthou et al., 2005). All experiments are listed in Table 1.

2.3. Gross Primary Production

The annual ice algal GPP integrated over depth, time, and area was calculated for each model grid cell from the simulated amount of carbon produced by sea-ice algae by photosynthesis for each ice layer. This GPP was multiplied by the time-evolving fraction of FYI per grid cell and integrated for 365 days to obtain the annual fast ice GPP.

3. Results and Discussion

3.1. Model Evaluation

This work focuses on 2005–2006 since total primary production by sea-ice algae has been estimated for that year in a previous study (Saenz & Arrigo, 2014). Only Davis Station provides a full-year time series of ice physical properties for 2005–2006, therefore we validate LIM1D with this data set. The model-simulated fast-ice thickness (in the NOSUB experiment) closely matches the observations (Figure 1b). The model run does not capture fast-ice breakout. This caveat, however, does not affect the estimated GPP, as production in a grid cell ceases when the satellite-based fast-ice product indicates fast-ice breakout in that cell (Figure 2a).

Simulated fast-ice primary production (Figure 2b; subgrid-scale mean = 0–65 mg C m^{-2} d^{-1}) agrees with the range reported in spring-time in situ primary production studies, for example, 0.5–85, 103 and 140 mg C m^{-2} d^{-1} for McMurdo Sound, Casey Station and Prydz Bay, respectively (Archer et al., 1996; Grossi et al., 1987; McMinn et al., 2012). Simulated phenology and observed ice-core-integrated Chl *a* values (IChla, [mg m^{-2}]; Meiners et al., 2018) of first-year fast ice algae near Davis, Syowa, and McMurdo Stations are shown in Figure 2c. They indicate a modest but important increase in biomass in autumn (in May) and a spring (onset in September/October and continued through to early December) algal bloom. The differences between the model and observations can partly be attributed to biases in ice-core GPP observations due to high spatial variability in ice-algal biomass and production (e.g., Lange et al., 2017) as well as the effects of grazing on ice algal biomass accumulation.

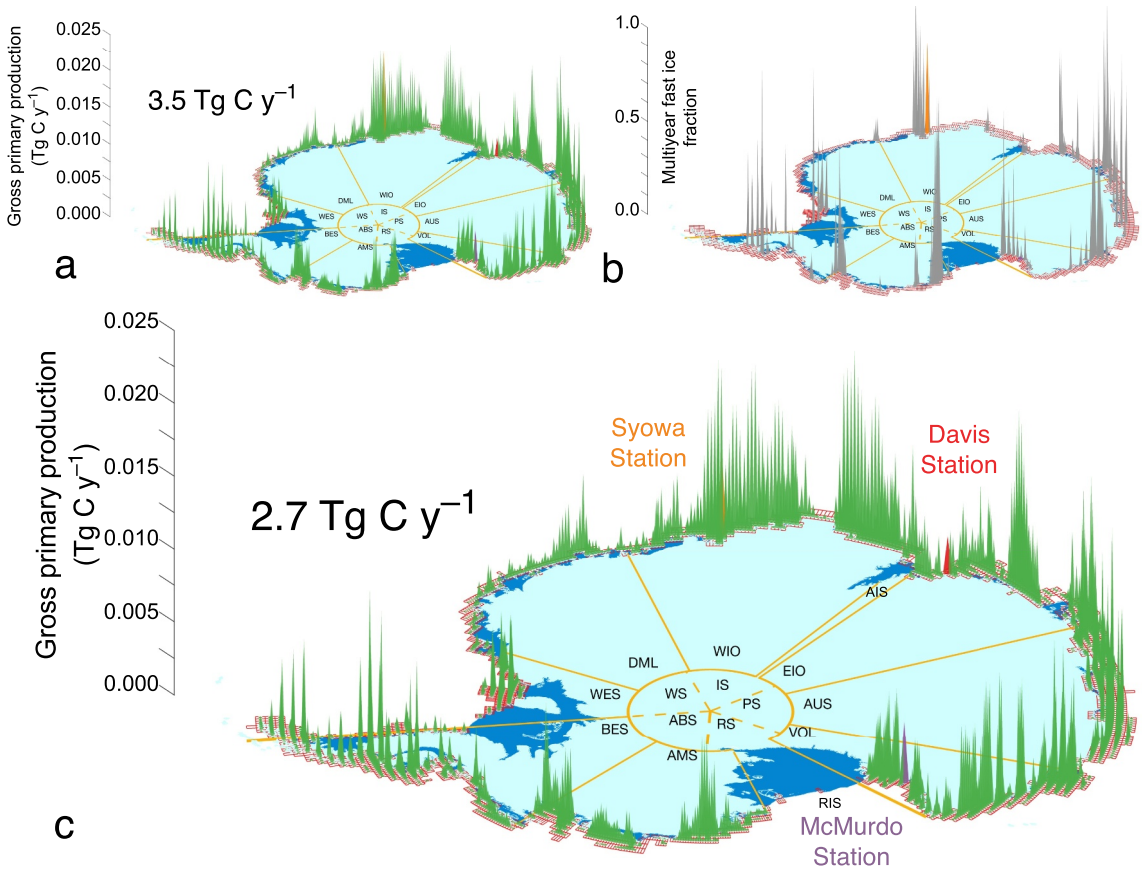

Figure 3. Gross primary production (GPP) in Antarctic landfast sea ice (K_{Si} = 50 μM or CONTROL). (a) Calculated by treating all ice pixels as first-year ice. (b) Fraction of multiyear ice area per grid cell. (c) GPP after subtracting the contribution from multiyear ice areas. The definitions for the abbreviations are shown in Table 2.

3.2. Fast Ice Primary Production in 2005–2006

Without masking MYI pixels, total fast-ice algal primary production estimates range from 1.5 to 5.7 Tg C y^{-1} (Figure 4). After subtracting the contribution from MYI areas (e.g., Figure 3 for CONTROL), fast-ice primary production reduces to 1.1–4.4 Tg C y^{-1} (Table 1). These estimates represent 5%–19% of the total 2005–2006 Southern Ocean sea-ice algal production (23.7 Tg C y^{-1}) as estimated by Saenz and Arrigo (2014). Hereafter, GPP without the MYI contribution is discussed. The mean GPP from all sensitivity runs is 2.75 ± 1.26 Tg C y^{-1} which is 12% ± 5% of the total sea-ice GPP (Saenz & Arrigo, 2014). The sector-by-sector fast-ice and sea-ice GPP estimates are summarized in Table 2. In the Bellingshausen Sea, mean fast-ice GPP is 0.32 ± 0.14 Tg C y^{-1}, which contributes 51% ± 22% to total sea-ice GPP in this sector (0.63 Tg C y^{-1}, Saenz & Arrigo, 2014). In East Antarctica, the Australian sector fast ice contributes 34 ± 19% to the total sea-ice GPP. The West Indian Ocean and Australian sectors display the highest fast-ice GPP, which can be explained by their relatively large fast-ice extent compared to other areas (Fraser et al., 2021). The high fast-ice contribution to total sea-ice GPP in the Bellingshausen Sea (up to 81%) highlights the importance of fast-ice production not only for Antarctic coastal ecosystems, but likely for wider areas where pack ice has been shown to disappear faster than fast ice. The correlation between fast-ice GPP and the fraction of overall sea ice that is fast ice was significant, with a Spearman correlation coefficient of 0.84 ($p = 0.005$), supporting the logical idea that ice area (habitat extent) is a key driver of total fast-ice algal production (Figure 5).

Our model suggests that Antarctic fast ice is annually more productive per unit area than pack ice. The ratio of simulated fast-ice GPP (this study) to that of pack ice (Saenz & Arrigo, 2014) for the widely used ocean sectors (Figure 6, Table 2) ranges from 2.2 to 6.9 (mean = 3.3, $N = 5$). Fast ice is generally more stable and stationary compared to pack ice, which, combined with the relatively thin snow atop (Fedotov et al., 1998), provides a more

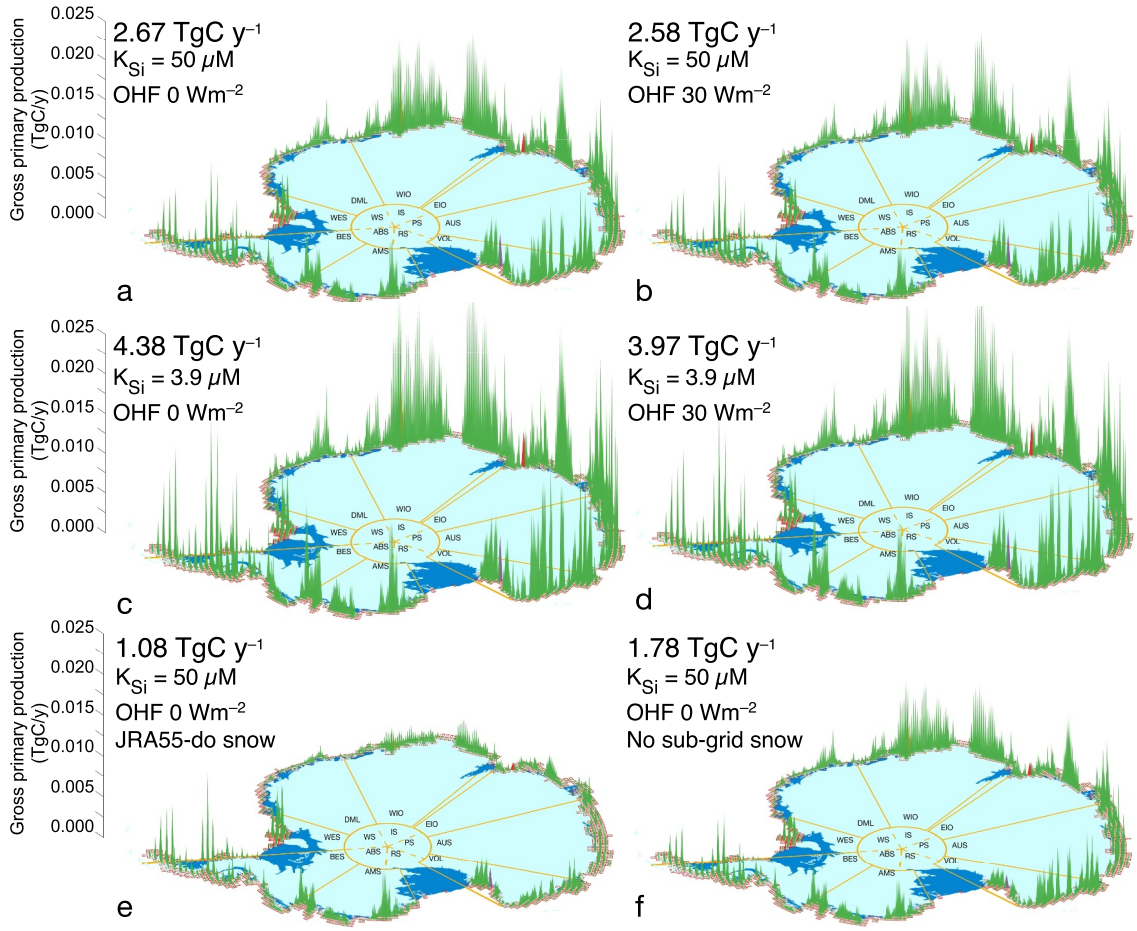

Figure 4. Spatial distribution of simulated annual fast ice algal production for all sensitivity experiments. (a) CONTROL (b) OHF (c) KSI (d) OHF_KSI (e) JRASNOW and (f) NOSUB (Table 1).

suitable environment for fast-ice algae to establish and thrive. Fast ice is also typically thicker and persists for longer than pack ice, providing a greater habitable volume and allowing more time for algae to grow within the ice matrix. Greater primary production in fast ice compared to pack ice is likely facilitated by higher macronutrient availability from coastal waters (van Leeuwe et al., 2018). Fast ice exhibits higher iron concentrations than pack ice, due to proximity to iron sources in coastal Antarctic areas (Lannuzel et al., 2016). Nutrients are also generally more abundant along the continental shelf, resulting in higher reservoirs of nutrients in fast ice relative to pack ice (Henley et al., 2023). These factors are potential explanations for the higher modeled annual productivity in Antarctic fast ice compared to pack ice, as modeled in this study.

3.3. Sensitivity of Fast-Ice Gross Primary Production

The majority of fast-ice algae reside in porous bottom layers of the ice where nutrient availability is high (Arrigo, 2016; Meiners et al., 2018). However, an improved understanding of ice algal community nutrient uptake dynamics, as well as their response to changing snow and ice cover thickness and duration, is needed to further constrain fast-ice primary production estimates. We tested the response of ice algae to oceanic heat flux, dissolved silicate uptake, snow thickness and air temperature forcings, as described in the following subsections.

Oceanic heat flux: We investigated the sensitivity of the model outputs by increasing oceanic heat flux to 30 W m^{-2} in the summer months (15 Nov—31 Dec 2005). This reduced the sea-ice growth season, hence the length of sea-ice algal production season and therefore the overall fast-ice GPP. A slight (<10%) decrease in the GPP was observed, from 4.38 to 3.97 Tg C y^{-1} (K_{Si} = 3.9 μM) and from 2.67 to 2.58 Tg C y^{-1} (K_{Si} = 50 μM or CONTROL).

Table 2
Sectorial Annual Ice Algal Gross Primary Production (Tg C)

Region	Fast ice mean GPP (SD)	Sea ice GPP (Saenz & Arrigo, 2014)	Fast ice/sea ice GPP (%) (SD)
Circumpolar	2.75 (1.26)	23.7	11.6 (5.3)
Dronning M. L.[a] (DML; 23°W–22.5°E)	0.07 (0.03)	5.27	1.3 (0.6)
West Ind. Ocean[a] (WIO; 22.5°–71°E)	0.64 (0.32)	3.12	20.4 (10.3)
Amery Ice Shelf[a] (AIS; 71°–74°E)	6.76 (3.67) × 10^{-4}	0.22	0.3 (0.2)
East Ind. Ocean (EIO; 74°–103°E)	0.28 (0.14)	1.16	24.3 (12.4)
Australia (AUS; 103°–146°E)	0.51 (0.28)	1.51	33.9 (18.7)
Vict. Oates L. (VOL; 146°–172°E)	0.47 (0.22)	1.44	32.4 (15.6)
Ross Ice Shelf[a] (RIS; 158°W–172°E)	1.57 (0.37) × 10^{-4}	2.81	0.0 (0.0)
Amundsen Sea (AMS; 102°–158°W)	0.24 (0.08)	2.90	8.3 (2.9)
Bellings. Sea (BES; 60°–102°W)	0.32 (0.14)	0.63	50.5 (21.8)
Weddell Sea[a] (WES; 23°–60°W)	0.22 (0.06)	4.68	4.8 (1.3)
Weddell Sector (WS; 60°W–20°E)	0.29 (0.08)	9.65	3.0 (0.8)
Indian Sector (IS; 20°–90°E)	0.84 (0.43)	4.36	19.3 (9.8)
Pacific Sector (PS; 90°–160°E)	0.79 (0.42)	2.53	31.0 (16.6)
Ross Sector (RS; 160°E−130°W)	0.35 (0.16)	5.76	6.1 (2.7)
Amundsen Bellings. Sector (ABS; 60°–130°W)	0.48 (0.19)	1.42	33.8 (13.6)

[a]Sectors were modified from Fraser et al. (2021) where DML (19° W–18° E), WIO (27° W–71° E) and WES (27°–60° E) and no AIS and RIS. SD is the standard deviation. Dronning M. L. is Dronning Maud Land, West Ind. Ocean is Western Indian Ocean, East Ind. Ocean is Eastern Indian Ocean, Vict. Oates L. is Victoria and Oates Lands, and Bellings. Sea is Bellingshausen Sea.

Dissolved silicate uptake: Most sea-ice algal communities in fast ice, particularly in biomass-rich bottom layers, are dominated by pennate diatoms that require DSi to build their frustules (e.g., van Leeuwe et al., 2018), making DSi concentrations potentially limiting (Lim et al., 2019). Sea-ice diatoms may have a much lower affinity for DSi than pelagic diatoms, with a K_{Si} value of 50 μM used in LIM1D producing the closest fit to both Chl *a* and DSi observations in fast ice collected near Davis Station (Lim et al., 2019). Moreover, Duarte et al. (2022) improved simulations of Chl *a* in an Arctic refrozen lead and second-year ice by increasing K_{Si} from 2.2 μM (Duarte et al., 2017) to 4 or 5 μM. The choice of K_{Si} may therefore strongly affect modeled GPP estimates in sea ice. Our study supports sensitivity to K_{Si} at the circum-Antarctic scale. Using K_{Si} = 3.9 μM (Sarthou et al., 2005) instead of 50 μM (Lim et al., 2019) increased the fast-ice GPP estimate by 39%. This increase in fast-ice GPP is much larger than the 14% reported by Saenz and Arrigo (2014) for a suite of sensitivity experiments exploring GPP sensitivity to complexity of ice algal habitat (2%), environmental forcings (13%), and nutrient availability (14%) while keeping a constant K_{Si} (60 μM). Combined, these findings highlight that K_{Si} is a key source of uncertainty for the estimation of circum-Antarctic sea-ice GPP.

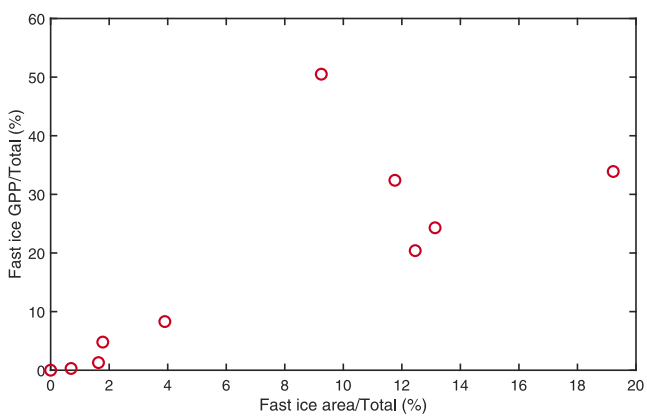

Figure 5. Correlation between fast-ice Gross Primary Production (GPP, %) and the fraction of overall sea ice that is fast ice with a Spearman correlation coefficient of 0.84 (p = 0.005) for sea ice sectors following Fraser et al. (2021).

Snow: Snow strongly affects both sea-ice growth and light supply to ice algae. Thin snow allows deeper penetration of photosynthetically active radiation, which results in earlier onset and greater sea-ice algal accumulation compared to a thicker snow cover (Figures 1a–1c). Abraham et al. (2015) showed that implementation of sub-grid scale snow thickness variability improves the model representation of light intensity at the bottom of the ice. Removing sub-grid scale variability of snow depth from model simulations (NOSUB) decreases the GPP by 33%. Without the fraction of each grid cell with a lower snow depth, as introduced by this procedure, there is later onset and lower intensity of light transmission to the bottom community, reducing productivity (Figures 1a–1c). Using the unrealistically heavy JRA55-do snowfall rate and distribution (JRASNOW) largely increases snow depth and reduces

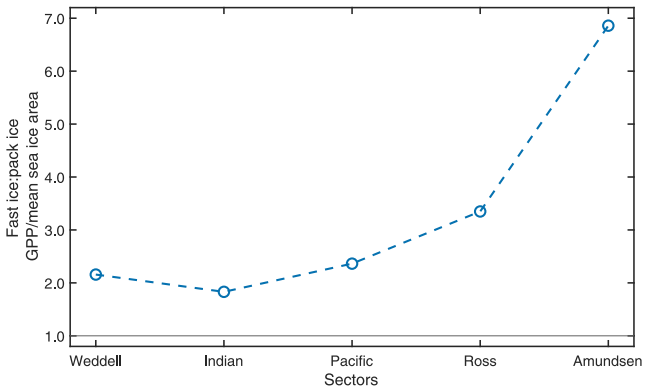

Figure 6. Area-normalized ration between Gross Primary Production (GPP) in fast ice versus pack ice for each sea ice sector following Saenz and Arrigo (2014).

the fast-ice GPP by 75%. These two experiments highlight the large impact of snow and its distribution on ice algal production (e.g., Jeffery et al., 2020), calling for further investigations on the impact of snow on fast-ice (and pack-ice) GPP.

Air temperature forcing: Using the JRA55-do air temperature (warmer in winter, Figure S1 in Supporting Information S1) reduced GPP from 2.67 to 2.38 Tg C y^{-1} (Table 1). The choice of air temperature forcing has less effect on GPP than dissolved silicate uptake and snow thickness (Section 3.3).

Altogether, the temporal progression of ice algal blooms in spring is linked to varying limiting factors with seasonally changing relative contributions (Arrigo, 2016; Arrigo et al., 1997; Campbell et al., 2015; Meiners et al., 2017). It is generally assumed that early in the season light limitation dominates. As sunlight increases, and ice algal growth progresses, nutrients (both silicate and nitrate) can become depleted thus limiting productivity (Henley et al., 2023; Lim et al., 2019). Due to its high albedo and light-attenuation properties, snow is a key factor in controlling the light available to ice-algal communities (Campbell et al., 2015; Leu et al., 2015). Note also that as biomass increases, self-shading can become an additional controlling factor. However, self-shading has been primarily reported from highly concentrated algal habitats, such as the sub-ice platelet layer (Arrigo et al., 1993), which were not included in our work. We note that the breakup of fast ice determined from Fraser et al. (2020)'s fast-ice distribution data set is the fundamental limitation of fast ice primary production for this model-based study (Figure 2).

Full-season fast-ice sampling has been conducted in very few Antarctic regions, and there is no existing data set with a comprehensive set of concomitant measurements of physical-chemical-biological variables from a platelet-ice free location (Carnat et al., 2014; Günther & Dieckmann, 1999). Existing data sets are generally short (<3 months), have a poor temporal (>1 week) resolution and are lacking key auxiliary physical observations such as snow data (Meiners et al., 2018). While studies like our modeling approach provide gap-filling information, high-resolution and full ice-season data sets of a suite of parameters are necessary to gain a deeper understanding of fast-ice algal temporal and spatial dynamics (Miller et al., 2015; Steiner et al., 2016).

3.4. Limitations and Future Modeling Work

Our first estimates of circum-Antarctic fast-ice GPP are likely conservative due to the complete exclusion of MYI (Sahashi et al., 2022) as well as biomass-rich platelet ice layer habitats (Arrigo et al., 1997). Platelet ice is a persistent feature in McMurdo Sound (Hoppmann et al., 2020; Langhorne et al., 2015), and harbors high and productive ice algal communities (Arrigo et al., 1993; van der Linden et al., 2020). Efforts to observe platelet ice distribution at regional scales are underway (Haas et al., 2021; Langhorne et al., 2023), as well as the development of a sub-ice platelet layer in a one-dimensional thermodynamic sea-ice model (Wongpan et al., 2021). Seasonal observations on oceanic heat flux under and near ice shelf cavities, needed to force these models, are however still lacking (McPhee et al., 2016). Given the importance of platelet ice in the Ross Sea and Weddell Sea sectors (Hoppmann et al., 2020; Langhorne et al., 2015), we assume that our model underestimates ice algal production in these areas, particularly in platelet-rich environments such as McMurdo Sound, along the Dronning Maud Land coast and other possible areas. Future work should include platelet ice layers and should also evaluate the inter-annual variability in fast-ice GPP, rather than focusing on a single year. Further studies focusing on evaluating the consequences of changes in fast ice area will help to understand impacts on coastal ecosystems. These will be particularly important given the recent changes observed in the Southern Ocean sea-ice and fast-ice extent (Fraser et al., 2023; Purich & Doddridge, 2023).

4. Conclusions

By combining new maps of fast ice with a one-dimensional sea-ice biogeochemical model, we provide a first estimate of fast-ice GPP and its relative contribution (12%) to overall Antarctic sea-ice primary productivity. Fast ice dominates the total sea-ice algal primary production in the Bellingshausen Sea. Our modeling approach underlines the need for integrated circum-Antarctic coastal observations and time-series data of oceanic heat flux, snow thickness, nutrient forcings and ice algal dynamics to further evaluate fast ice algal and biogeochemical

models, and optimize sea-ice algal growth parameterizations. Future work should focus on interannual variability in the context of recent climate induced changes in the Southern Ocean sea-ice extent and include the quantification of the contribution of platelet ice algal communities.

Data Availability Statement

LIM1D is available at http://forge.ipsl.jussieu.fr/lim1d revision #3.26. Reanalysis data used to force the model: JRA55-do accessed via Tsujino et al. (2018) and ERA5 (Hersbach et al., 2018) were downloaded from the Copernicus Climate Change Service using the Climate Data Store API (https://doi.org/10.24381/cds.adbb2d47). Figures were produced using Antarctic Mapping Tools for MATLAB (Greene et al., 2017) and cmocean colormap (Thyng et al., 2016). Fast-ice distribution (Fraser et al., 2020) is available at https://doi.org/10.26179/5d267d1ceb60c. Data presented here is available via the Australian Antarctic Data Centre (Wongpan, 2024).

Acknowledgments
This project was supported through the Australian Government as part of the Antarctic Science Collaboration Initiative program and contributes to Project 6 (Sea Ice) of the Australian Antarctic Program Partnership (project ID ASCI000002). DL is supported by the Australian Research Council through a Future Fellowship (FT190100688). ADF is supported by ARC Grants FT230100234, LP170101090, LE220100103 and DP240100325. ADF and PW acknowledge the generous support of the Harris Charitable Trust through the Antarctic Science Foundation. PW is also supported by the Australian Research Council's Special Research Initiative for Antarctic Gateway Partnership (Project ID SR140300001). SM received funding from the Research Council of Norway (RCN) for the project "I-CRYME: Impact of CRYosphere Melting on Southern Ocean Ecosystems and biogeochemical cycles" (Grant 335512) and for the Norwegian Centre of Excellence "iC3: Center for ice, Cryosphere, Carbon and Climate" (Grant 332635) and from the European Union for the project "WOBEC: Weddell Sea Observatory and Biodiversity and Ecosystem Change" (Grant 350906). Davis sea ice thickness data was supported by Antarctic Science Advisory Committee (ASAC) Project 1328. This work also contributes to the Australian Research Council Special Research Initiative, Australian Centre for Excellence in Antarctic Science (Project Number SR200100008) and Australian Antarctic Science project #4546. This research was supported by using the Nectar Research Cloud and by the Tasmanian Partnership for Advanced Computing. The Nectar Research Cloud is a collaborative Australian research platform supported by the National Collaborative Research Infrastructure Strategy-funded Australian Research Data Commons (ARDC). We also thank the Scientific Committee on Antarctic Research (SCAR)-, Surface Ocean - Lower Atmosphere Study (SOLAS)- and World Climate Research Programme (WCRP)-Climate and Cryosphere (CliC)-funded working group on Biogeochemical Exchange Processes at the Sea Ice Interfaces (BEPSII) for setting the ground for discussions and building projects among the sea ice biogeochemistry community. We thank the editor and two anonymous reviewers for their insightful comments on an earlier version of the manuscript. Open access publishing facilitated by University of Tasmania, as part of the Wiley - University of Tasmania agreement via the Council of Australian University Librarians.

References

Abraham, C., Steiner, N., Monahan, A., & Michel, C. (2015). Effects of subgrid-scale snow thickness variability on radiative transfer in sea ice. *Journal of Geophysical Research: Oceans*, *120*(8), 5597–5614. https://doi.org/10.1002/2015jc010741

Aoki, S. (2017). Breakup of land-fast sea ice in Lützow-Holm Bay, East Antarctica, and its teleconnection to tropical Pacific sea surface temperatures. *Geophysical Research Letters*, *44*(7), 3219–3227. https://doi.org/10.1002/2017gl072835

Archer, S. D., Leakey, R. J. G., Burkill, P. H., Sleigh, M. A., & Appleby, C. J. (1996). Microbial ecology of sea ice at a coastal Antarctic site: community composition, biomass and temporal change. *Marine Ecology Progress Series*, *135*, 179–195. https://doi.org/10.3354/meps135179

Arrigo, K. R. (2016). Sea ice as a habitat for primary producers. In *Sea ice* (pp. 352–369). https://doi.org/10.1002/9781118778371.ch14

Arrigo, K. R., Kremer, J. N., & Sullivan, C. W. (1993). A simulated Antarctic fast ice ecosystem. *Journal of Geophysical Research*, *98*(C4), 6929–6946. https://doi.org/10.1029/93jc00141

Arrigo, K. R., van Dijken, G. L., & Bushinsky, S. (2008). Primary production in the Southern Ocean, 1997–2006. *Journal of Geophysical Research*, *113*(C8), C08004. https://doi.org/10.1029/2007jc004551

Arrigo, K. R., Worthen, D. L., Lizotte, M. P., Dixon, P., & Dieckmann, G. (1997). Primary production in Antarctic sea ice. *Science*, *276*(5311), 394–397. https://doi.org/10.1126/science.276.5311.394

Campbell, K., Mundy, C. J., Barber, D. G., & Gosselin, M. (2015). Characterizing the sea ice algae chlorophyll a–snow depth relationship over Arctic spring melt using transmitted irradiance. *Journal of Marine Systems*, *147*, 76–84. https://doi.org/10.1016/j.jmarsys.2014.01.008

Carnat, G., Zhou, J., Papakyriakou, T., Delille, B., Goossens, T., Haskell, T., et al. (2014). Physical and biological controls on DMS,P dynamics in ice shelf-influenced fast ice during a winter-spring and a spring-summer transitions. *Journal of Geophysical Research: Oceans*, *119*(5), 2882–2905. https://doi.org/10.1002/2013jc009381

DeJong, H. B., Dunbar, R. B., & Lyons, E. A. (2018). Late summer Frazil ice-associated algal blooms around Antarctica. *Geophysical Research Letters*, *45*(2), 826–833. https://doi.org/10.1002/2017gl075472

Duarte, P., Assmy, P., Campbell, K., & Sundfjord, A. (2022). The importance of turbulent ocean–sea ice nutrient exchanges for simulation of ice algal biomass and production with CICE6.1 and Icepack 1.2. *Geoscientific Model Development*, *15*(2), 841–857. https://doi.org/10.5194/gmd-15-841-2022

Duarte, P., Meyer, A., Olsen, L. M., Kauko, H. M., Assmy, P., Rösel, A., et al. (2017). Sea ice thermohaline dynamics and biogeochemistry in the Arctic Ocean: Empirical and model results. *Journal of Geophysical Research: Biogeosciences*, *122*(7), 1632–1654. https://doi.org/10.1002/2016jg003660

Fedotov, V. I., Cherepanov, N. V., & Tyshko, K. P. (1998). Some features of the growth, structure and metamorphism of East Antarctic landfast sea ice. In *Antarctic Sea ice: Physical processes, interactions and variability* (pp. 343–354). https://doi.org/10.1029/AR074p0343

Fogt, R. L., Sleinkofer, A. M., Raphael, M. N., & Handcock, M. S. (2022). A regime shift in seasonal total Antarctic sea ice extent in the twentieth century. *Nature Climate Change*, *12*(1), 54–62. https://doi.org/10.1038/s41558-021-01254-9

Fraser, A. D., Massom, R. A., Handcock, M. S., Reid, P., Ohshima, K. I., Raphael, M. N., et al. (2021). Eighteen-year record of circum-Antarctic landfast-sea-ice distribution allows detailed baseline characterisation and reveals trends and variability. *The Cryosphere*, *15*(11), 5061–5077. https://doi.org/10.5194/tc-15-5061-2021

Fraser, A. D., Massom, R. A., Ohshima, K. I., Willmes, S., Kappes, P. J., Cartwright, J., & Porter-Smith, R. (2020). High-resolution mapping of circum-Antarctic landfast sea ice distribution, 2000–2018. *Earth System Science Data*, *12*(4), 2987–2999. https://doi.org/10.5194/essd-12-2987-2020

Fraser, A. D., Wongpan, P., Langhorne, P. J., Klekociuk, A. R., Kusahara, K., Lannuzel, D., et al. (2023). Antarctic landfast sea ice: A review of its physics, biogeochemistry and ecology. *Reviews of Geophysics*, *61*(2), e2022RG000770. https://doi.org/10.1029/2022rg000770

Greene, C. A., Gwyther, D. E., & Blankenship, D. D. (2017). Antarctic mapping Tools for Matlab. *Computers & Geosciences*, *104*, 151–157. https://doi.org/10.1016/j.cageo.2016.08.003

Grossi, S. M., Kottmeier, S. T., Moe, R. L., Taylor, G. T., & Sullivan, C. W. (1987). Sea ice microbial communities. VI. Growth and primary production in bottom ice under graded snow cover. *Marine Ecology Progress Series*, *35*, 153–164. https://doi.org/10.3354/meps035153

Günther, S., & Dieckmann, G. S. (1999). Seasonal development of algal biomass in snow-covered fast ice and the underlying platelet layer in the Weddell Sea, Antarctica. *Antarctic Science*, *11*(3), 305–315. https://doi.org/10.1017/s0954102099000395

Haas, C., Langhorne, P. J., Rack, W., Leonard, G. H., Brett, G. M., Price, D., et al. (2021). Airborne mapping of the sub-ice platelet layer under fast ice in McMurdo Sound, Antarctica. *The Cryosphere*, *15*(1), 247–264. https://doi.org/10.5194/tc-15-247-2021

Heil, P. (2006). Atmospheric conditions and fast ice at Davis, East Antarctica: A case study. *Journal of Geophysical Research*, *111*(C5). https://doi.org/10.1029/2005jc002904

Heil, P., Allison, I., & Lytle, V. I. (1996). Seasonal and interannual variations of the oceanic heat flux under a landfast Antarctic sea ice cover. *Journal of Geophysical Research*, *101*(C11), 25741–25752. https://doi.org/10.1029/96jc01921

Henley, S. F., Cozzi, S., Fripiat, F., Lannuzel, D., Nomura, D., Thomas, D. N., et al. (2023). Macronutrient biogeochemistry in Antarctic land-fast sea ice: Insights from a circumpolar data compilation. *Marine Chemistry*, *257*, 104324. https://doi.org/10.1016/j.marchem.2023.104324

Hersbach, H., Bell, B., Berrisford, P., Biavati, G., Horányi, A., Muñoz Sabater, J., et al. (2018). ERA5 hourly data on single levels from 1979 to present. *Copernicus Climate Change Service (C3S) Climate Data Store (CDS)*. https://doi.org/10.24381/cds.adbb2d47

Hoppmann, M., Richter, M. E., Smith, I. J., Jendersie, S., Langhorne, P. J., Thomas, D. N., & Dieckmann, G. S. (2020). Platelet ice, the Southern Ocean's hidden ice: A review. *Annals of Glaciology*, *61*(83), 341–368. https://doi.org/10.1017/aog.2020.54

Inall, M. E., Brearley, J. A., Henley, S. F., Fraser, A. D., & Reed, S. (2022). Landfast ice controls on turbulence in Antarctic coastal seas. *Journal of Geophysical Research: Oceans*, *127*(1), e2021JC017963. https://doi.org/10.1029/2021jc017963

Jeffery, N., Maltrud, M. E., Hunke, E. C., Wang, S., Wolfe, J., Turner, A. K., et al. (2020). Investigating controls on sea ice algal production using E3SMv1.1-BGC. *Annals of Glaciology*, *61*(82), 51–72. https://doi.org/10.1017/aog.2020.7

Kohlbach, D., Lange, B. A., Schaafsma, F. L., David, C., Vortkamp, M., Graeve, M., et al. (2017). Ice algae-produced carbon is critical for overwintering of Antarctic krill Euphausia superba. *Frontiers in Marine Science*, *4*, 310. https://doi.org/10.3389/fmars.2017.00310

Lange, B. A., Katlein, C., Castellani, G., Fernández-Méndez, M., Nicolaus, M., Peeken, I., & Flores, H. (2017). Characterizing spatial variability of ice algal chlorophyll a and net primary production between sea ice habitats using horizontal profiling platforms. *Frontiers in Marine Science*, *4*, 349. https://doi.org/10.3389/fmars.2017.00349

Langhorne, P. J., Haas, C., Price, D., Rack, W., Leonard, G. H., Brett, G. M., & Urbini, S. (2023). Fast ice thickness distribution in the Western Ross Sea in late spring. *Journal of Geophysical Research: Oceans*, *128*(2), e2022JC019459. https://doi.org/10.1029/2022jc019459

Langhorne, P. J., Hughes, K. G., Gough, A. J., Smith, I. J., Williams, M. J. M., Robinson, N. J., et al. (2015). Observed platelet ice distributions in Antarctic sea ice: An index for ocean-ice shelf heat flux. *Geophysical Research Letters*, *42*(13), 5442–5451. https://doi.org/10.1002/2015gl064508

Lannuzel, D., Vancoppenolle, M., van der Merwe, P., de Jong, J., Meiners, K. M., Grotti, M., et al. (2016). Iron in sea ice: Review and new insights. *Elementa: Science of the Anthropocene*, *4*. https://doi.org/10.12952/journal.elementa.000130

Large, W. G., & Yeager, S. G. (2004). Diurnal to decadal global forcing for ocean and sea-ice models: The data sets and flux climatologies. In *National center for atmospheric research boulder*.

Legendre, L., Ackley, S., Dieckmann, G., Gulliksen, B., Horner, R., Hoshiai, T., et al. (1992). Ecology of sea ice biota. *Polar Biology*, *12*(3–4), 429–444. https://doi.org/10.1007/bf00243114

Leu, E., Mundy, C. J., Assmy, P., Campbell, K., Gabrielsen, T. M., Gosselin, M., et al. (2015). Arctic spring awakening – Steering principles behind the phenology of vernal ice algal blooms. *Progress in Oceanography*, *139*, 151–170. https://doi.org/10.1016/j.pocean.2015.07.012

Lim, S. M., Moreau, S., Vancoppenolle, M., Deman, F., Roukaerts, A., Meiners, K. M., et al. (2019). Field observations and physical-biogeochemical modeling suggest low silicon affinity for Antarctic fast ice diatoms. *Journal of Geophysical Research: Oceans*, *124*(11), 7837–7853. https://doi.org/10.1029/2018jc014458

Louw, S. D. V., Walker, D. R., & Fawcett, S. E. (2022). Factors influencing sea-ice algae abundance, community composition, and distribution in the marginal ice zone of the Southern Ocean during winter. *Deep Sea Research Part I: Oceanographic Research Papers*, *185*, 103805. https://doi.org/10.1016/j.dsr.2022.103805

McMinn, A., Ashworth, C., Bhagooli, R., Martin, A., Salleh, S., Ralph, P., & Ryan, K. (2012). Antarctic coastal microalgal primary production and photosynthesis. *Marine Biology*, *159*(12), 2827–2837. https://doi.org/10.1007/s00227-012-2044-0

McMinn, A., Pankowskii, A., Ashworth, C., Bhagooli, R., Ralph, P., & Ryan, K. (2010). In situ net primary productivity and photosynthesis of Antarctic sea ice algal, phytoplankton and benthic algal communities. *Marine Biology*, *157*(6), 1345–1356. https://doi.org/10.1007/s00227-010-1414-8

McPhee, M. G., Stevens, C. L., Smith, I. J., & Robinson, N. J. (2016). Turbulent heat transfer as a control of platelet ice growth in supercooled under-ice ocean boundary layers. *Ocean Science*, *12*(2), 507–515. https://doi.org/10.5194/os-12-507-2016

Meiners, K. M., Arndt, S., Bestley, S., Krumpen, T., Ricker, R., Milnes, M., et al. (2017). Antarctic pack ice algal distribution: Floe-scale spatial variability and predictability from physical parameters. *Geophysical Research Letters*, *44*(14), 7382–7390. https://doi.org/10.1002/2017gl074346

Meiners, K. M., Vancoppenolle, M., Carnat, G., Castellani, G., Delille, B., Delille, D., et al. (2018). Chlorophyll-a in Antarctic landfast sea ice: A first synthesis of historical ice core data. *Journal of Geophysical Research: Oceans*, *123*(11), 8444–8459. https://doi.org/10.1029/2018jc014245

Miller, L. A., Fripiat, F., Else, B. G. T., Bowman, J. S., Brown, K. A., Collins, R. E., et al. (2015). Methods for biogeochemical studies of sea ice: The state of the art, caveats, and recommendations. *Elementa: Science of the Anthropocene*, *3*, 000038. https://doi.org/10.12952/journal.elementa.000038

Moreau, S., Vancoppenolle, M., Delille, B., Tison, J.-L., Zhou, J., Kotovitch, M., et al. (2015). Drivers of inorganic carbon dynamics in first-year sea ice: A model study. *Journal of Geophysical Research: Oceans*, *120*(1), 471–495. https://doi.org/10.1002/2014jc010388

Parkinson, C. L. (2019). A 40-y record reveals gradual Antarctic sea ice increases followed by decreases at rates far exceeding the rates seen in the Arctic. *Proc Natl Acad Sci U S A*, *116*(29), 14414–14423. https://doi.org/10.1073/pnas.1906556116

Pinkerton, M. H., Boyd, P. W., Deppeler, S., Hayward, A., Höfer, J., & Moreau, S. (2021). Evidence for the impact of climate change on primary producers in the Southern Ocean. *Frontiers in Ecology and Evolution*, *9*, 592027. https://doi.org/10.3389/fevo.2021.592027

Pinkerton, M. H., & Hayward, A. (2021). Estimating variability and long-term change in sea ice primary productivity using a satellite-based light penetration index. *Journal of Marine Systems*, *221*, 103576. https://doi.org/10.1016/j.jmarsys.2021.103576

Purich, A., & Doddridge, E. W. (2023). Record low Antarctic sea ice coverage indicates a new sea ice state. *Communications Earth & Environment*, *4*(1), 314. https://doi.org/10.1038/s43247-023-00961-9

Quetin, L. B., Ross, R. M., Frazer, T. K., & Haberman, K. L. (1996). Factors affecting distribution and abundance of zooplankton, with an emphasis on Antarctic krill, Euphausia superba. *Antarctic Research Series*, *70*, 357–371. https://doi.org/10.1029/AR070p0357

Raphael, M. N., & Handcock, M. S. (2022). A new record minimum for Antarctic sea ice. *Nature Reviews Earth & Environment*, *3*(4), 215–216. https://doi.org/10.1038/s43017-022-00281-0

Roukaerts, A., Deman, F., Van der Linden, F., Carnat, G., Bratkic, A., Moreau, S., et al. (2021). The biogeochemical role of a microbial biofilm in sea ice. *Elementa: Science of the Anthropocene*, *9*(1), 00134. https://doi.org/10.1525/elementa.2020.00134

Saenz, B. T., & Arrigo, K. R. (2014). Annual primary production in Antarctic sea ice during 2005-2006 from a sea ice state estimate. *Journal of Geophysical Research: Oceans*, *119*(6), 3645–3678. https://doi.org/10.1002/2013jc009677

Sahashi, R., Nomura, D., Toyota, T., Tozawa, M., Ito, M., Wongpan, P., et al. (2022). Effects of snow and remineralization processes on nutrient distributions in multi-year Antarctic landfast sea ice. *Journal of Geophysical Research: Oceans*, *127*(7), e2021JC018371. https://doi.org/10.1029/2021jc018371

Sarthou, G., Timmermans, K. R., Blain, S., & Tréguer, P. (2005). Growth physiology and fate of diatoms in the ocean: A review. *Journal of Sea Research*, *53*(1–2), 25–42. https://doi.org/10.1016/j.seares.2004.01.007

Steiner, N. S., Bowman, J., Campbell, K., Chierici, M., Eronen-Rasimus, E., Falardeau, M., et al. (2021). Climate change impacts on sea-ice ecosystems and associated ecosystem services. *Elementa: Science of the Anthropocene*, *9*(1), 00007. https://doi.org/10.1525/elementa.2021.00007

Steiner, N. S., Deal, C., Lannuzel, D., Lavoie, D., Massonnet, F., Miller, L. A., et al. (2016). What sea-ice biogeochemical modellers need from observers. *Elementa: Science of the Anthropocene*, *4*, 000084. https://doi.org/10.12952/journal.elementa.000084

Swadling, K. M. (1998). *Influence of seasonal ice formation on life cycle strategies of Antarctic copepods*. University of Tasmania. Retrieved from https://eprints.utas.edu.au/22306/

Thyng, K., Greene, C., Hetland, R., Zimmerle, H., & DiMarco, S. (2016). True colors of oceanography: Guidelines for effective and accurate colormap selection. *Oceanography*, *29*(3), 9–13. https://doi.org/10.5670/oceanog.2016.66

Tsujino, H., Urakawa, L. S., Griffies, S. M., Danabasoglu, G., Adcroft, A. J., Amaral, A. E., et al. (2020). Evaluation of global ocean–sea-ice model simulations based on the experimental protocols of the Ocean Model Intercomparison Project phase 2 (OMIP-2). *Geoscientific Model Development*, *13*(8), 3643–3708. https://doi.org/10.5194/gmd-13-3643-2020

Tsujino, H., Urakawa, S., Nakano, H., Small, R. J., Kim, W. M., Yeager, S. G., et al. (2018). JRA-55 based surface dataset for driving ocean–sea-ice models (JRA55-do). *Ocean Modelling*, *130*, 79–139. https://doi.org/10.1016/j.ocemod.2018.07.002

Ushio, S. (2006). Factors affecting fast-ice break-up frequency in Lützow-Holm Bay, Antarctica. *Annals of Glaciology*, *44*, 177–182. https://doi.org/10.3189/172756406781811835

Vancoppenolle, M., Goosse, H., de Montety, A., Fichefet, T., Tremblay, B., & Tison, J.-L. (2010). Modeling brine and nutrient dynamics in Antarctic sea ice: The case of dissolved silica. *Journal of Geophysical Research*, *115*(C2). https://doi.org/10.1029/2009jc005369

Vancoppenolle, M., Meiners, K. M., Michel, C., Bopp, L., Brabant, F., Carnat, G., et al. (2013). Role of sea ice in global biogeochemical cycles: Emerging views and challenges. *Quaternary Science Reviews*, *79*, 207–230. https://doi.org/10.1016/j.quascirev.2013.04.011

Vancoppenolle, M., & Tedesco, L. (2016). Numerical models of sea ice biogeochemistry. In *Sea ice* (pp. 492–515). https://doi.org/10.1002/9781118778371.ch20

van der Linden, F. C., Tison, J. L., Champenois, W., Moreau, S., Carnat, G., Kotovitch, M., et al. (2020). Sea ice CO2 dynamics across Seasons: Impact of processes at the Interfaces. *Journal of Geophysical Research: Oceans*, *125*(6), e2019JC015807. https://doi.org/10.1029/2019jc015807

van Leeuwe, M. A., Tedesco, L., Arrigo, K. R., Assmy, P., Campbell, K., Meiners, K. M., et al. (2018). Microalgal community structure and primary production in Arctic and Antarctic sea ice: A synthesis. *Elementa: Science of the Anthropocene*, *6*, 4. https://doi.org/10.1525/elementa.267

Wongpan, P. (2024). Gross primary production of Antarctic landfast sea ice: A model-based estimate. *Australian Antarctic Data Centre*. https://doi.org/10.26179/707g-2159

Wongpan, P., Meiners, K. M., Langhorne, P. J., Heil, P., Smith, I. J., Leonard, G. H., et al. (2018). Estimation of Antarctic land-fast sea ice algal biomass and snow thickness from under-ice radiance Spectra in two contrasting areas. *Journal of Geophysical Research: Oceans*, *123*(3), 1907–1923. https://doi.org/10.1002/2017jc013711

Wongpan, P., Vancoppenolle, M., Langhorne, P. J., Smith, I. J., Madec, G., Gough, A. J., et al. (2021). Sub-ice platelet layer physics: Insights from a mushy-layer sea ice model. *Journal of Geophysical Research: Oceans*, *126*(6), e2019JC015918. https://doi.org/10.1029/2019jc015918

References From the Supporting Information

Shine, K. P., & Henderson-Sellers, A. (1985). The sensitivity of a thermodynamic sea ice model to changes in surface albedo parameterization. *Journal of Geophysical Research*, *90*(D1), 2243–2250. https://doi.org/10.1029/JD090iD01p02243